

EMBEDDED FBG SENSORS AND AWG-BASED WAVELENGTH INTERROGATOR FOR HEALTH MONITORING OF COMPOSITE MATERIALS

Shinji Komatsuzaki*, Seiji Kojima*, Akihito Hongo*, Nobuo Takeda **, and Tateo Sakurai***

*Hitachi Cable, Ltd, **The University of Tokyo,

***R&D Institute of Metals and Composites for Future Industries

Keywords: FBG, AWG, Small-diameter optical fiber, health monitoring, composite material

Abstract

We have been developing a health monitoring system for composites. It excites and receives Lamb waves propagating through the structures made of composites. The PZT actuators and Embedded FBG sensors in this system are used as transmitters and receivers of Lamb waves. Various kinds of damages can be detected from the change in the received waveforms. We developed a small-diameter optical fiber with a large relative index difference (Δ) for the embedded FBG sensors and wavelength interrogator based on an arrayed waveguide grating to detect changes in the Bragg wavelength of the sensors due to the reception of Lamb waves. A small-diameter optical fiber with large Δ can not only be embedded in the composites without inducing any defects but also the fiber itself is not deteriorated by the embedding. The wavelength interrogator has no mechanical moving parts and it is suitable for detecting high-speed changes in wavelengths.

1 Introduction

Composite materials have useful properties such as being light in weight and mechanically tough. Because of these advantages they are beginning to replace metals especially in aerospace fields to reduce weight and thus save energy. Although they have these advantages, the complex process of failure originating in their structure has been an obstacle to their extended use. Delamination or debonding is typical damage that occurs in composite materials. These can occur in the material due to fatigue or impact sustained by the structure. This invisible damage grows within composite materials and finally leads to catastrophic failures. Present aircraft structures are designed not to lead

to complete failure to prevent such accidents even if there is some degree of unseen damage, by using large amounts of composite materials¹⁾. This clearly does not take the full advantage of composite materials. Much time and attention is given during the inspection process so that damage is not overlooked. There is therefore an urgent demand for a health monitoring system that can effectively be used to detect unseen damage.

We have been developing the FBG/PZT hybrid sensing system²⁾⁻⁴⁾ for this purpose. It is an active sensing system that detects various kinds of damages from the change in the waveforms of Lamb waves excited and received by the system. The PZT actuators and embedded FBG sensors in the system are used to excite and receive Lamb waves. This report describes a small-diameter optical fiber for embedded FBG sensors, and an arrayed waveguide grating (AWG) based wavelength interrogator that is used to detect the changes in the Bragg wavelength of FBG sensors as a result of the reception of Lamb waves.

2 System composition

Our FBG/PZT hybrid sensing system (Fig. 1) is composed of PZT actuators, a signal generator, a high-speed amplifier driving the PZT actuators, embedded FBG sensors, a wavelength interrogator, and a computer.

The Lamb waves excited by the PZT actuators travel through the structure of the composite material and change the wavelengths of the light reflected by the FBG sensors. The wavelength changes are detected by the wavelength interrogator and sent to the computer where they are stored and analyzed to determine whether damage has occurred or not.

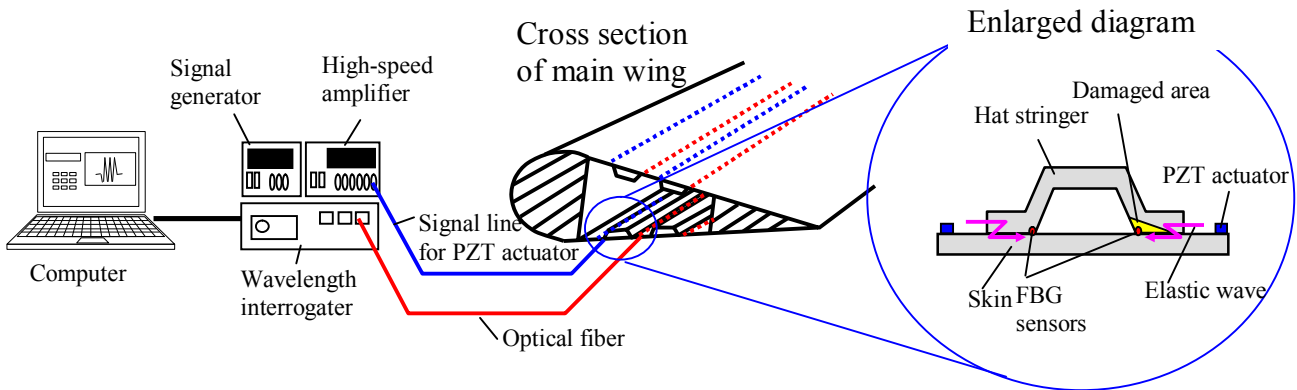


Fig. 1 Schematic of FBG/PZT hybrid sensing system

3. AWG-based wavelength interrogator

3.1 Principal

The wavelength interrogator (Fig. 2) is composed of a broadband light source, an optical circulator, an AWG with a temperature controller, O/E converters for the output ports of the AWG, and two AD converters. The broadband light first enters the FBG sensor, and the light whose wavelength corresponds to the Bragg wavelength of the sensor is reflected at the sensor and is fed into the AWG via the optical circulator. The AWG has many output ports, each of which transmits light with a different wavelength, as shown in Fig. 3. The wavelength spacing between the adjacent output ports are all the same. When the Bragg wavelength of the sensor is situated between the center wavelengths of two adjacent output ports, the reflected light is divided between those two ports. If the Bragg wavelength changes, the divided power ratio also changes. Consequently, the change

in the Bragg wavelength is converted into output power changes for those two adjacent output ports. This conversion ratio (sensitivity) strongly depends on the relationship between the initial Bragg wavelength and the center wavelengths of the output ports of the AWG as shown in Fig. 4. The horizontal axis here plots the relative displacement ratio of the initial Bragg wavelength to the spacing width of the center wavelengths of the output ports from the midpoint, and the vertical axis plots the attenuation rate of the sensitivity from the maximum value. The sensitivity reaches maximum when the initial Bragg wavelength is at the midpoint between two adjacent output ports, and reaches minimum when the initial Bragg wavelength coincides with the center wavelength of an output port. The sensitivity, at minimum, decreases to only 5 % of the maximum value. Therefore, the initial Bragg wavelength should be adjusted to the midpoint of two adjacent output ports to enable precise measurement. This condition is obtained by using the temperature

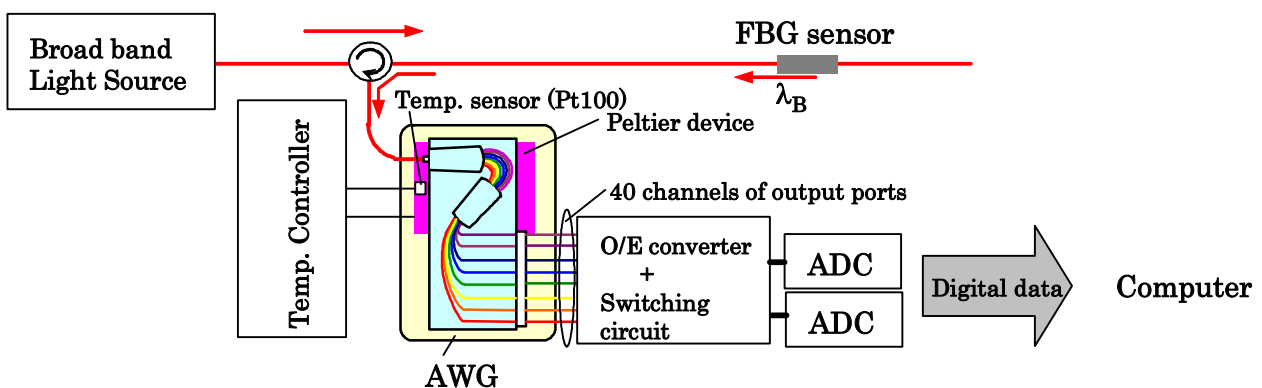


Fig. 2 Schematic of AWG-based wavelength interrogator

controller to adjust the center wavelengths of the output ports. The O/E converters convert the lights from the two output ports into electric signals, the AD converters convert them to digital signals, and the computer acquires them. The rate of data acquisition is 10 mega samples per a second.

We fabricated the damage detection device combining the signal generator and the wavelength interrogator. There is a photograph of it in Fig. 5. The size is $50 \times 30 \times 15$ cm.

3. 2 Frequency characteristic

We evaluated the frequency characteristics of the damage detection device by measuring the waveforms of Lamb waves with frequencies from 100 kHz to 1 MHz. The experimental setup is outlined in Fig. 6. A PZT actuator and an FBG sensor were bonded 10 mm apart on a CFRP laminated plate. The input signal waves to the PZT actuator and the received waveforms are shown in Fig. 7. The signal waves inputted to the PZT actuator were three cycles of sine waves filtered through a Hamming window. Each received waveform was the average of 10,000 waveforms. It took 10 seconds for averaging. We were able to detect the elastic waves with frequencies of 100 kHz to 1 MHz very clearly.

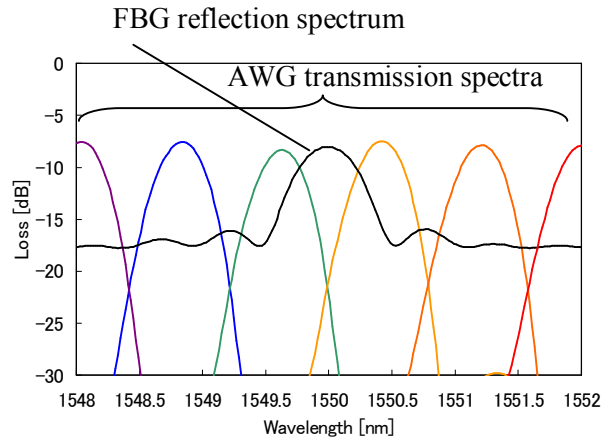


Fig. 3 Transmission spectra for AWG and reflection spectrum for FBG

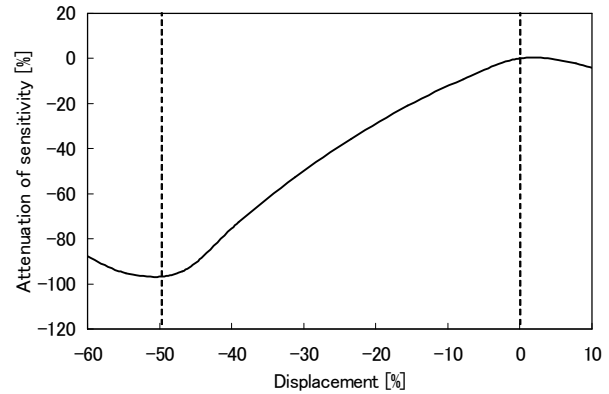


Fig. 4 Dependence of sensitivity on initial Bragg wavelength

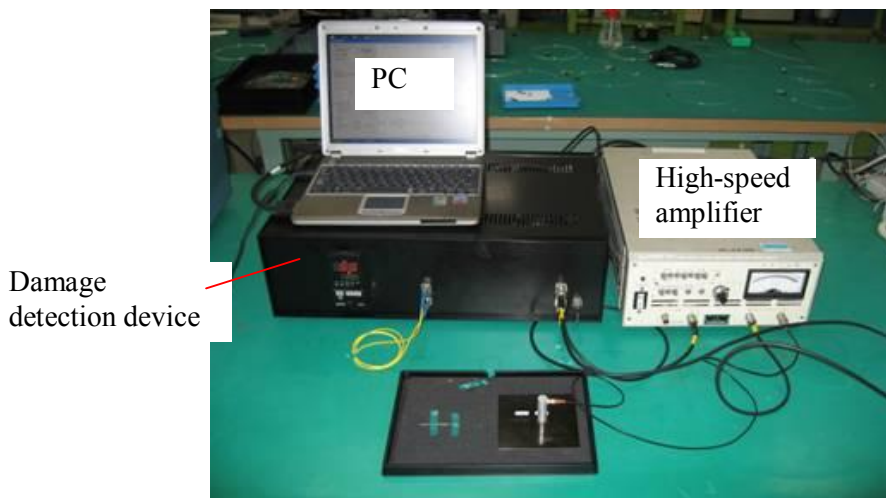


Fig. 5 Photograph of damage detection device

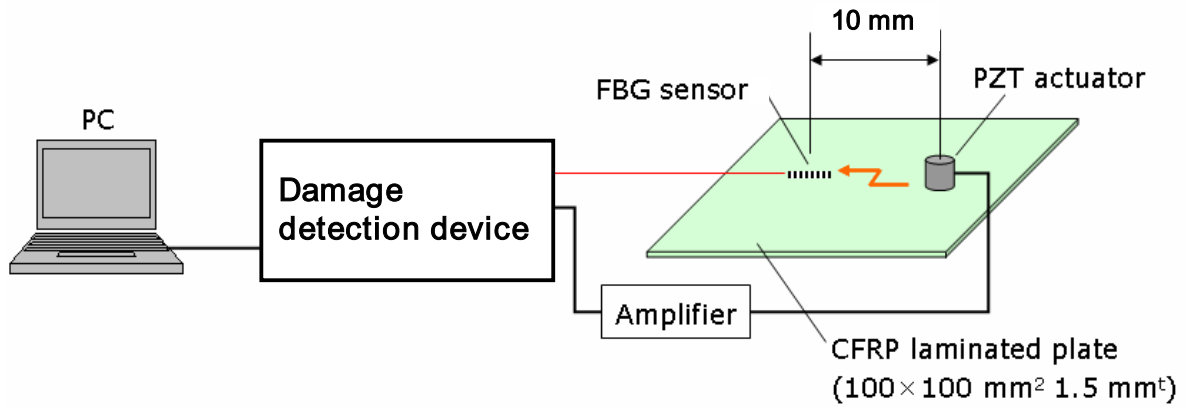


Fig. 6 Experimental setup for evaluating frequency characteristics

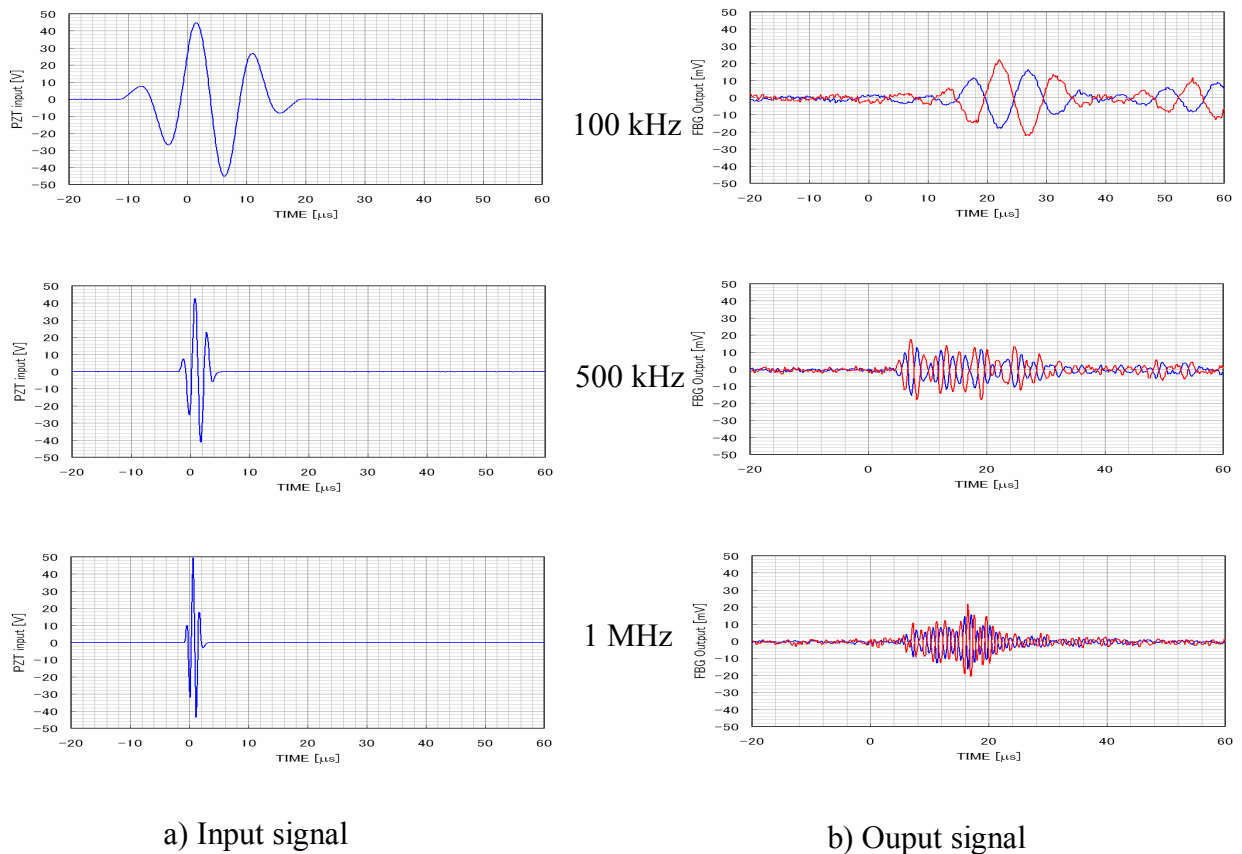


Fig. 7 Input and output waveforms

4 Small-diameter optical fiber

4.1 Features

We developed a small-diameter optical fiber for embedded FBG sensors. There is a cross-sectional view of the small-diameter optical fiber Fig. 8. The diameter of its cladding is 40 μm and whole diameter including the coating is 52 μm . The small-diameter optical fiber is so thin that it can be embedded in the composite materials without inducing any defects in them.

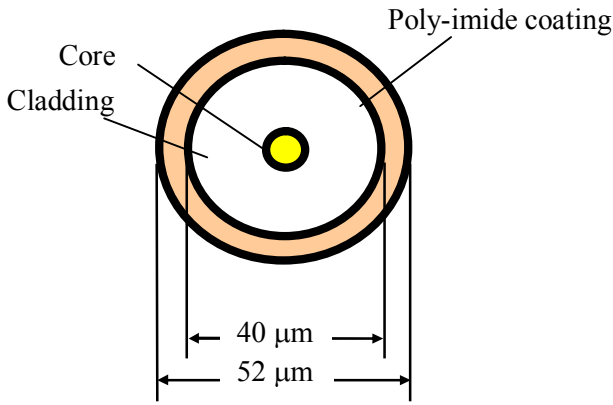


Fig. 8 Cross section of small-diameter optical fiber

4.2 Small-diameter optical fiber with large relative index difference

Care must be taken under embedded condition regarding loss increase in the fiber due to the micro bending caused by lateral pressure. The micro bending loss can be expressed as

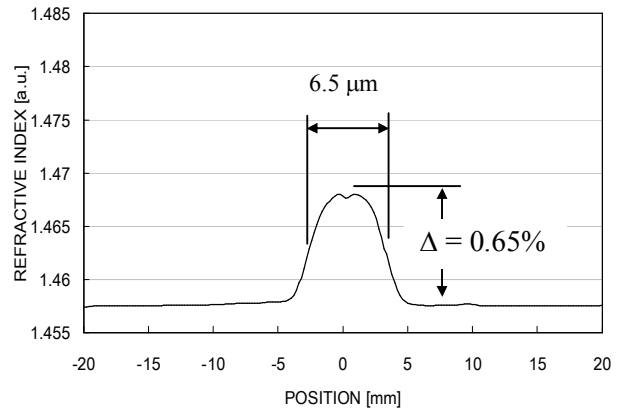
$$\alpha_m \propto \frac{a^4}{\Delta^3 b^6} \quad (1)$$

where, a is the radius of the core, b is the diameter of the cladding, and Δ is the relative index difference between the optical fiber's core and cladding. It is clear from this formula that the larger the relative index difference between the core and the cladding, the more loss increase due to micro-bending can be suppressed. The relative index difference Δ is defined by

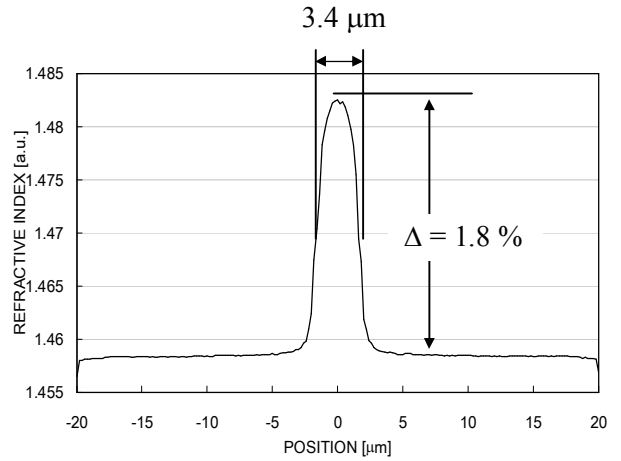
$$\Delta \propto \frac{n_{\text{core}} - n_{\text{clad}}}{n_{\text{core}}} \quad (2)$$

where, n_{core} is the refractive index of the core and n_{clad} is the refractive index of the cladding.

We have been using a small-diameter optical fiber with a Δ of 0.65% which is higher than typical Δ for normal single-mode optical fiber (0.35%). However, as this value is not practical, we experienced large embedment loss. We fabricated the fiber with a Δ of 1.8%. The refractive index profiles of the small-diameter optical fiber with the Δ of 0.65 % and 1.8 % are shown in Fig.3. We also reduced the core diameter to allow the fiber to be operated in the single mode.



a) $\Delta = 0.65\%$



b) $\Delta = 1.8\%$

Fig. 9 Refractive index profiles of small-diameter optical fiber

4. 3 Connecting technique

As the small-diameter optical fiber was fragile and hard to handle. Therefore, outside the composite material, the small-diameter optical sensor should be connected to a normal single-mode optical fiber with a cladding diameter of $125\ \mu\text{m}$ outside the composite material, making it easy to handle and enabling it to be connected to the measuring apparatus. We fabricated a special ferrule made of zirconia ceramic. The end faces of a small-diameter and a normal single-mode optical fiber that were inserted into the ferrule and a standard MU ferrule are shown in Fig. 10.

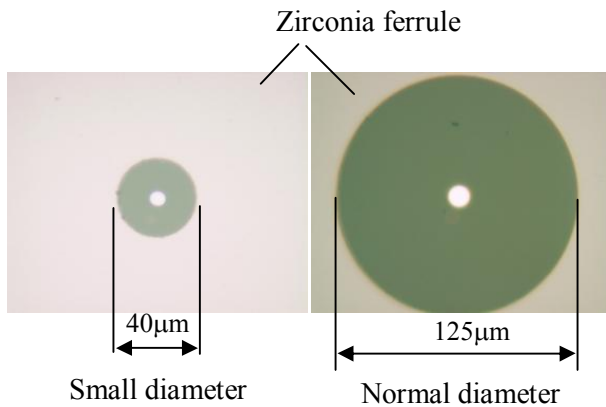


Fig. 10 End faces of small- and normal-diameter optical fiber inserted in zirconia ferrules

The inner diameter of the special ferrule was $40 +3-0\ \mu\text{m}$. We chemically removed the layer around the end of the optical fiber before we inserted it into

the ferrule, taking the thickness deviation of the polyimide coating layer, which has an average thickness of $6\ \mu\text{m}$, into consideration. This special ferrule was compatible with the simplified MU plug's ferrule. We fabricated the small-diameter optical fiber module shown in Fig. 11 for embedding use. MU simplified plugs using the special ferrules were installed at the both ends. SUS tubes whose inner diameters were $900\ \text{mm}$ were also installed with the simplified MU plugs for protection and to facilitate easier handling. This module could easily be connected to the normal single-mode optical fiber cord with MU plug easily, using a commercially available receptacle.

4. 4 Connection loss and embedment loss

We evaluated the embedment loss of the small-diameter optical fiber and the connection loss of the simplified MU plug using the special ferrule for the small-diameter optical fiber, with the set up shown in Fig. 12. We prepared 20 small-diameter optical fiber modules with a Δ of 0.65 % and 1.8 % (10 modules for 0.65 % and 10 modules for 1.8 %), and embedded them in the bonding layer between CFRP laminated plates. The embedment length was 10 cm. We measured the insertion loss of the modules before and after embedment by using the setup shown in Fig. 13. Both ends of the small-diameter optical fiber modules were connected to normal single-mode optical fibers, and the transmitted power from an ASE light source was measured with an optical power meter. We defined connection loss of the simplified MU plug with the special ferrule as

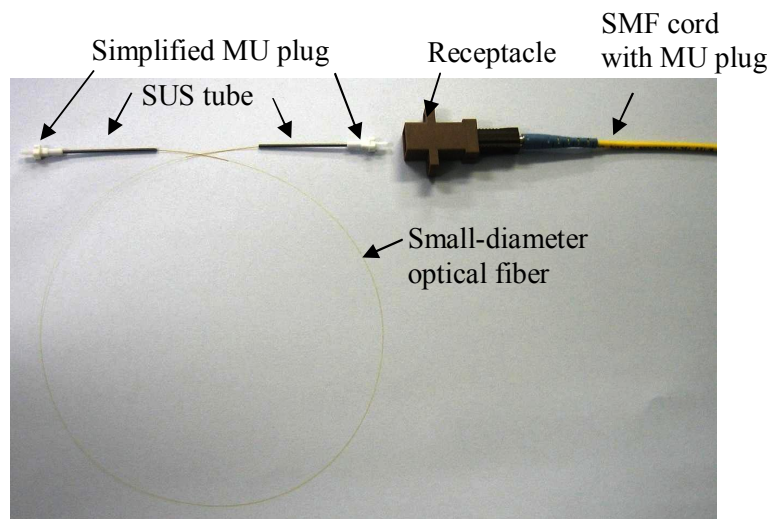


Fig 11 Small-diameter optical fiber module

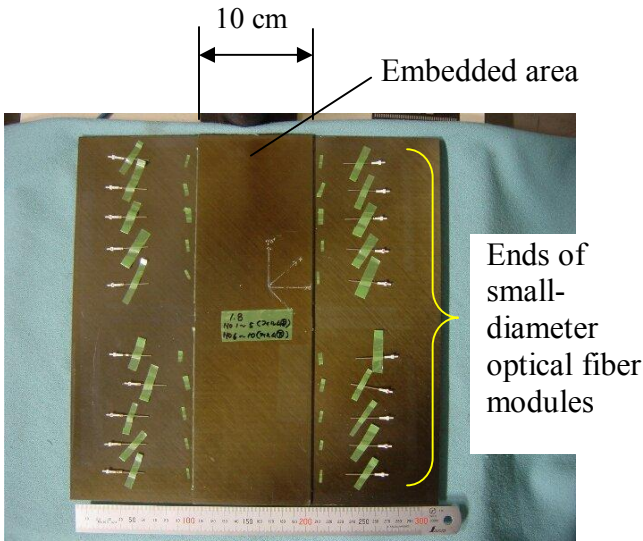


Fig. 12 Setup for evaluating embedment loss and connection loss

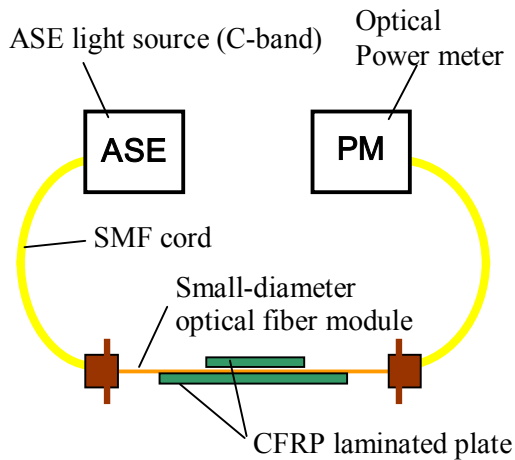


Fig. 13 Setup for measuring insertion loss

a half of the insertion loss of the small-diameter optical fiber module, and embedment loss as the increase in insertion loss due to embedment. The connection losses and embedment loss we obtained are shown in the histograms in Figs. 14 and 15. The average connection losses were 1.6 dB for the 0.65 % fiber and 2.1 dB for the 1.8 % fiber. Because of the small diameter of the core (therefore small mode field diameter), the connection loss for the 1.8 % fiber was larger than that for the 0.65 % fiber. The embedment loss for the 1.8 % fiber, on the other hand, was 0.09 dB/cm on average, and this was much smaller than that for 0.65 % fiber (0.42

dB/cm). The total loss can be expressed as the sum of double the connection loss and embedment loss and it is clear that it depends on the embedment length according to which fiber is suitable for suppressing total loss, 0.65 % or 1.8 %. The calculation of total loss using the average connection losses and embedment losses revealed that if the embedment length was more than 3 cm, the larger Δ fiber was better (1.5 cm for an FBG sensor because light is reflected at the grating and makes a round trip).

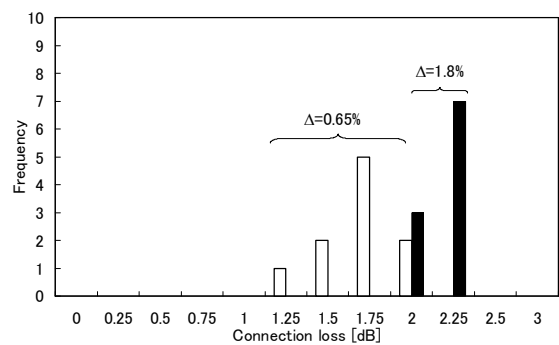


Fig. 14 Connection loss

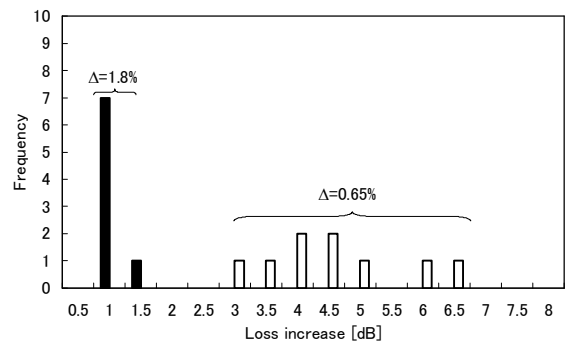


Fig. 15 Embedment loss (loss increase due to embedment)

5 Conclusion

We developed a device to detect damage by combining an AWG-based wavelength interrogator and a signal generator. We confirmed that this device could detect the Lamb waves up to 1 MHz.

We also developed a small-diameter optical fiber with large relative index difference (1.8 %) and a special connector that enabled the small-diameter optical fiber to be connected to a normal single-mode optical fiber. These can improve the total

optical loss in the system where the embedment length is longer than 1.5 cm.

6 Acknowledgements

This work was conducted as a part of the “Civil Aviation Fundamental Technology Program - Advanced Materials & Process Development for Next-Generation Structures” project under contract with the R&D Institute of Metals and Composites for Future Industries (RIMCOF), funded by Ministry of Economy, Trade and Industry (METI) of Japan.

We would like to thank Mr. Toshimichi Ogisu of Fuji Heavy Industries, Ltd. for his cooperation with the experiments.

References

- [1] M. Chun-Yung Niu, “Composite Airframe Structures, Practical Design Information and Data”, Conmilit Press Ltd., Hong Kong, 1997
- [2] S. Kojima, A. Hongo, S. Komatsuzaki, and N. Takeda, “High-speed optical wavelength interrogator using a PLC-type optical filter for fiber Bragg grating sensors” SPIE’s International symposium on Smart Structures and Materials, Proceeding of SPIE Vol.5384, pp. 241–249, 2004
- [3] S. Komatsuzaki, S. Kojima, A. Hongo, N. Takeda, and T. Sakurai, “Development of high-speed optical wavelength interrogation system for damage detection in composite materials”, SPIE International symposium on Smart Structures and Materials, Proceeding of SPIE Vol.5758, pp. 54–61, 2005
- [4] S. Komatsuzaki, S. Kojima, A. Hongo, N. Takeda, and T. Sakurai, “Development of small-diameter optical fiber sensors and high-speed optical wavelength interrogator for damage detection in composite materials,” SPIE International Symposium on Smart Structures and Materials, Proceedings of SPIE, Vol. 6167, pp. 616703–1– 616703–8, 2006